Optik 125 (2014) 3134–3137

Contents lists available at ScienceDirect

Optik

journal homepage: www.elsevier.de/ijleo

Transmission characteristics of a microscale dielectric slab waveguide device with a deep groove and an embedded metallodielectric grating at low terahertz frequency

Teguh P. Negara [a,b], Husin Alatas [a,c,*], Agah D. Garnadi [a,d], Sri Nurdiati [d]

[a] Research Cluster for Dynamics and Modeling of Complex Systems, Faculty of Mathematics and Natural Sciences, Bogor Agricultural University, Jl. Meranti, Kampus IPB Darmaga, Bogor 16680, Indonesia
[b] Department of Computer Science, Pakuan University, Bogor, Indonesia
[c] Theoretical Physics Division, Department of Physics, Bogor Agricultural University, Jl. Meranti, Kampus IPB Darmaga, Bogor 16680, Indonesia
[d] Computational Mathematics Division, Department of Mathematics, Bogor Agricultural University, Jl. Meranti, Kampus IPB Darmaga, Bogor 16680, Indonesia

ARTICLE INFO

Article history:
Received 19 June 2013
Accepted 15 December 2013

Keywords:
Slab waveguide
Metallodielectric grating
FDTD method
UPML boundary condition

ABSTRACT

We discuss the transmission characteristics of a microscale dielectric waveguide device with a deep groove and an embedded metallodielectric grating illuminated by a continuous wave of TM and TE modes at low terahertz frequency. To study its performance we solve numerically the corresponding Maxwell equations by means of finite difference time domain method with uniaxial perfectly match layer as its boundary condition. By varying the angle of incident, grating filling factor and refractive index of analyte in the deep groove, it is found that the device exhibits a significant transmission enhancement for the TM mode due to the existence of surface plasmon interaction. We also demonstrate its potential application as a biosensor device.

1. Introduction

Photonics structure with embedded metallic materials has been widely used in integrated optical devices due to the existence of propagating surface plasmon (SP) at the interface between metal and dielectric materials [1]. Its presence is highly sensitive with respect to the environment changes. Physically, the existence of this phenomenon can be explained as a consequence of a collective oscillation of electrons at the metal-dielectric interface due to transverse magnetic (TM) electromagnetic mode which leads to a large enhancement of electric field around the corresponding interface [1,2]. This enhancement is strongly depends on the surrounding of the related metallic structure. Obviously, this phenomenon can be applied as a sensing platform [3]. In general, the application of SP is widely considered in biosensing devices such as for cell, protein and bacterial detection such as based on long-range surface plasmon waveguide [4,5] and metallic grating [6].

Indeed, beside its use for biosensing platform, this phenomenon can also be applied for other puposes. It was recently reported in Ref. [7] that SP has been used to assist a Cu_xO photocatalyst to split pure water for H_2 gas production more rapidly. In the meantime, it has also been used to detect the presence of H_2 itself by replacing a cladding segment of an optical fiber with metallic layer as reported in Ref. [8] or using photonic crystal fiber [9].

A photonic structure, namely, a dielectric slab waveguide structure with embedded metallic grating has also been considered to be used for such purposes [10–13]. This structure was shown to have specific performance due to the combination effect of grating and SP properties that could lead to enhanced transmission characteristics [13].

Based on the abovementioned facts, in this paper we discuss the results of our systematic numerical investigation on the performance of a specific microscale photonic structure in the form of a dielectric slab waveguide device with metallodielectric grating embedded on its top, and a deep groove which is assumed to be filled by an analyte. We illuminate the system by continuous electromagnetic waves of TM and TE modes and choose their operational frequency in low terahertz order which is related to the resonance of the most protein vibrational frequencies [14]. Solving the associated Maxwell equations by means of standard finite difference time domain (FDTD) method incorporated with uniaxial perfectly matched layer (UPML) [15] as the corresponding boundary condition, we investigate numerically the transmission characteristics of the corresponding modes with respect to the

* Corresponding author at: Research Cluster for Dynamics and Modeling of Complex Systems, Faculty of Mathematics and Natural Sciences, Bogor Agricultural University Jl. Meranti, Kampus IPB Darmaga, Bogor 16680, Indonesia.
E-mail address: alatas@ipb.ac.id (H. Alatas).

0030-4026/$ – see front matter © 2014 Published by Elsevier GmbH.
http://dx.doi.org/10.1016/j.ijleo.2013.12.015

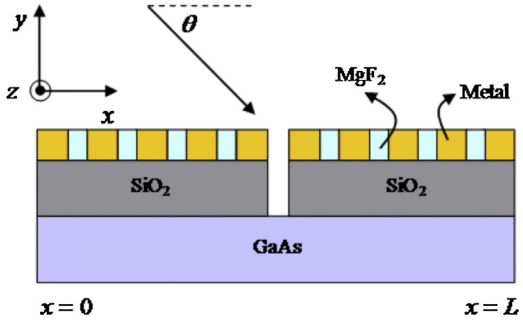

Fig. 1. Sketch of the corresponding microscale dielectric slab waveguide with metallodielectric grating and a deep groove in the middle. (For interpretation of the references to colour in this figure legend, the reader is referred to the web version of this article.)

variation of angle of incident, grating filling factor and refractive index of analyte in the deep groove. It is found that the transmission of the electric field is significantly affected by the variation of those parameters, specifically for the TM cases. The device shows sensitive response with respect to the variation of analyte refractive index, so that it can be potentially functioned as an optical sensor. For comparison, we also consider the case of fully dielectric grating structure.

This paper is organized as follows. Discussion on the device structure and the related numerical formulation is given in section two, followed by a discussion about the result of the conducted numerical calculation in Section 3. This paper is summarized in Section 4.

2. Device structure and numerical method

As illustrated in Fig. 1, the considered device consists of a GaAs substrate with refractive index of $n = 3.61$, thickness of $h = 30\ \mu m$ and length of $L = 300\ \mu m$, two finite SiO_2 slab waveguides with $n = 1.45$, $h = 39\ \mu m$ and $L = 2 \times 145\ \mu m$ as well as a metallodielectric grating embedded on top of the slab waveguide with fix periodicity of $\Lambda = 31\ \mu m$, $h = 21\ \mu m$, and the metal permittivity is given by drude model [16]:

$$\varepsilon(\nu) = 1 - \frac{1.52 \times 10^{30}}{\nu(\nu - 1.6 \times 10^{13} i)} \tag{1}$$

where ν is the operational frequency in Hz. The width of metallic section is denoted by w which is a parameter to be varied, whereas the dielectric section of width $\Lambda - w$ is filled by MgF_2 with $n = 1.38$. The two slab waveguides are separated by a deep groove with the same $\Lambda - w$ width but $h = 51\ \mu m$ depth. The device is illuminated by an oblique continuous wave with angle of incident from normal to perpendicular is denoted by θ. The grating filling factor is defined as:

$$f = 1 - \frac{w}{\Lambda} \tag{2}$$

Here, to investigate the significant effect of SP, we set f to be relatively far less than one.

Here, we consider the TM (TE) wave case where $\vec{E}(\vec{H})$ field lies in the x–y plane, and the $\vec{H}(\vec{E})$ field lies in the z axis. The associated Maxwell equations are solved numerically by means of the FDTD method incorporated with UPML boundary condition which is represented by an artificial anisotropic absorbing material layer. Compare to the other types of PML boundary conditions, this boundary condition shows a better efficiency when handling the oblique constinuous waves. Detailed formulation of the corresponding FDTD and UPML can be found in Ref. [15].

The dynamical characteristics of electromagnetic wave propagation inside such a complex photonics system strongly depend on its material as well as the related structure. In most cases, these material and structural properties interact each other to perform an emergent behavior which is difficult to predict (semi-) analytically. Therefore, an *ab initio* investigation based on full numerical calculation is needed to explore the possible allowed phenomenon. The used of FDTD with UPML boundary condition is aimed to conduct this. For the corresponding numerical calculation, we consider the number of mesh to be 492×226 with size $\Delta x = \Delta y = 1\ \mu m$, and the time increment is chosen to be $\Delta t = 1.67\ fs$. The initial and final observation time after the steady condition reached are set to $t_i = 4.5$ ps and $t_f = 5.0$ ps, respectively.

To characterize the transmission performance of the device, we consider the transmission enhancement factor at specific angle of incident θ defined as follows:

$$\Gamma = \frac{\int_{t_i}^{t_f} \left(\int_0^h \left| \vec{E}\left(x = L,\ y,\ t;\ \theta\right) \right|^2 dy \right) dt}{\int_{t_i}^{t_f} \left(\int_0^h \left| \vec{E}_0\left(x = L,\ y,\ t;\ \theta = 0\right) \right|^2 dy \right) dt} \tag{3}$$

here, the parameters L and h denote the device total length and SiO_2 slab waveguide thickness, respectively. The functions $\vec{E}(L,\ y,\ t;\ \theta)$ and $\vec{E}_0\left(L,\ y,\ t;\ \theta = 0\right)$ are the transmitted electric fields at oblique and normal incident, respectively, while the parameters t_i and t_f denote the aforementioned initial and final observation times.

3. Transmission characteristics

We first investigate the characteristics of Γ parameter given by Eq. (3) with respect to the variation of angle of incident in the range of $0 \le \theta \le 90^\circ$. This parameter describes the ratio between the field intensity at $x = L$ for various angle of incident with respect to that of normal incident. We choose the operational frequency at $\nu = 5$ THz, while the grating filling factor is set to be of $f = 0.032$ which is equal to the slit of 1 μm and the deep groove is filled by MgF_2. The numerical calculation results of these parameters for the cases of TE and TM modes are given in Fig. 2 a. It is remarkable that an almost similar trend but with relatively large difference in its value is found for both modes where $\Gamma_{TM} > \Gamma_{TE}$. Clearly, the enhancement is getting larger for increasing angle of incident. The highest Γ_{TM} is observed at $\theta = 85^\circ$ while $\theta = 90^\circ$ is for Γ_{TE}. The difference of Γ parameter $\Delta\Gamma = \Gamma_{TM} - \Gamma_{TE}$ is shown in Fig. 2b. To compare the performance characteristics of the considered device, we also conduct investigation for the case in which the corresponding metal in the grating is replaced by SiO_2 material, and the result is given in Fig. 3. As expected, although still share similar trend with the metallic case, but less enhancement factor is found for this case as well as less difference between the TM and TE cases.

To further characterize the device performance at $\theta = 85^\circ$, we calculate Γ for various operational frequency ν, namely, in the range of $\nu = 1$– 10 THz, and the results are given in Fig. 4. It is found that Γ exhibits high values at $\nu = 4$ and 8 THz, while in all range the average difference between TM and TE is still relatively large.

We suspect that the origin of this large difference between TE and TM cases is actually due to the effect of SP of TM mode. To prove this, we calculate the Γ variation as a function of grating filling factor (f) at fix $\theta = 85^\circ$. Given in Fig. 5 is the corresponding characteristics for $\nu = 5$ and 8 THz. It is shown that Γ tends to increase exponentially when f decreases, so that the distance between the two adjacent metal-dielectric interfaces in the associated grating is getting shorter. Depicted in Fig. 6 is the TM mode electric field intensity distribution for $\theta = 85^\circ$ and $f = 0.032$. Without loss of generality we only draw for the case of $\nu = 5$ THz. It is demonstrated

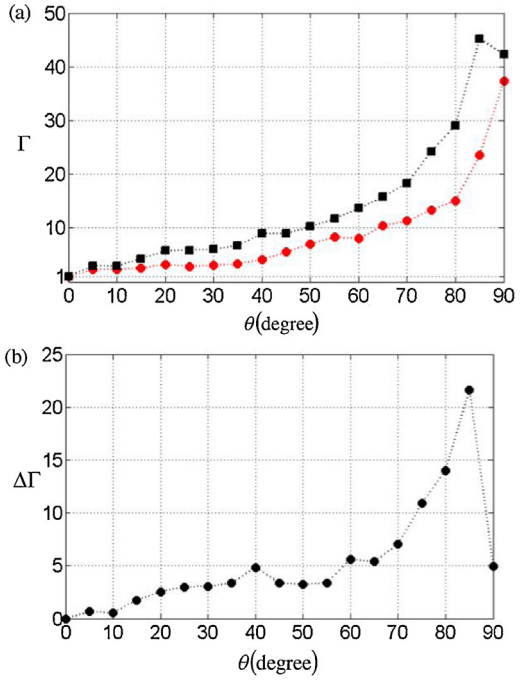

Fig. 2. (a) $\Gamma(\theta)$ of TM (black-square) and TE (red-circle) for $f = 0.032$ (b) difference between $\Gamma_{TM}(\theta)$ and $\Gamma_{TE}(\theta)$. (For interpretation of the references to colour in this figure legend, the reader is referred to the web version of this article.)

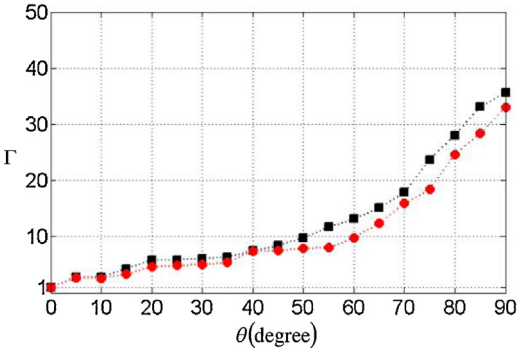

Fig. 3. $\Gamma(\theta)$ of TM (black-square) and TE (red-circle) at $f = 0.032$ for the case of fully dielectric grating where the metal is replaced by SiO_2. (For interpretation of the references to colour in this figure legend, the reader is referred to the web version of this article.)

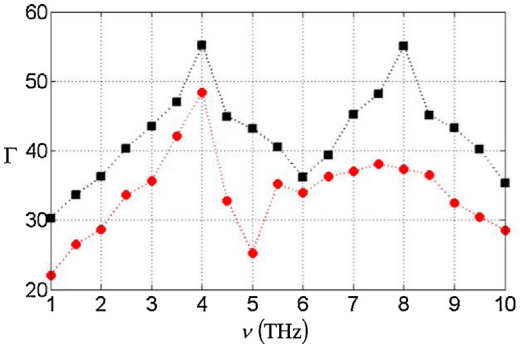

Fig. 4. Spectral characteristic at low THz frequency of $\Gamma(\theta = 85^\circ)$ for TM (black-square) and TE (red-circle) modes. (For interpretation of the references to colour in this figure legend, the reader is referred to the web version of this article.)

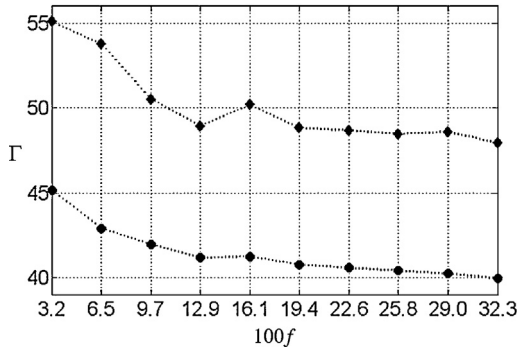

Fig. 5. Variation of $\Gamma(\theta = 85^\circ)$ with respect to the variation of filling factor (f) for TM mode at $\nu = 5$ THz (black-circle) and 8 THz (black-diamond).

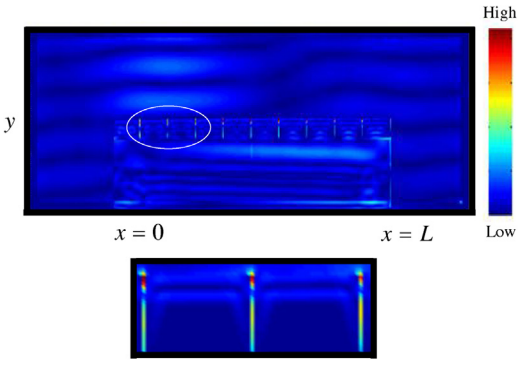

Fig. 6. Field distribution of TM mode at $\theta = 85^\circ$ and its zoom (below picture) showing the existence of SP. (For interpretation of the references to colour in this figure legend, the reader is referred to the web version of this article.)

for this case that the field around the associated metal–dielectric interfaces is enhanced significantly indicating the existence of the SP interaction, while it is not the case for the TE mode. Clearly, the related distance seems adequate to enhance the interaction between the two adjacent SPs. This result obviously supports our hypothesis regarding the role of SP in the metallodielectric grating case.

To complete our investigation, we also calculate the device characteristics by varying the refractive index of analyte that fills the deep groove as shown in Fig. 1 for $\nu = 5$ and 8 THz cases. This characteristic is of important if one consider the related device to be used as a sensor. The result is shown in Fig. 7. In this calculation. the Γ expression given by Eq. (3) is considered as the ratio between electric field intensity at $\theta = 85^\circ$ and $\theta = 0^\circ$ with $f = 0.032$ for the same refractive index of analyte. As expected, we found a linear response of Γ with respect to the variation of refractive index $1.3 \leq n \leq 1.4$.

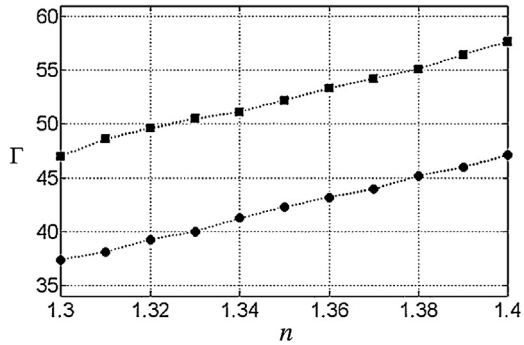

Fig. 7. Response characteristic of $\Gamma(\theta = 85^\circ)$ with respect to analyte refractive index (n) variation at $\nu = 5$ THz (black-circle) and 8 THz (black-diamond).

It is found that the sensitivity for cases of $\nu = 5$ THz and $\nu = 8$ THz exhibit a similar characteristic, although the value of Γ of the later case is relatively far larger than the former one as shown in Fig. 4. It is important to emphasize that this sensitivity characteristic may not generally valid for all frequencies considered and in order to improve it one should consult to a more rigorous semi-analytic method such as couple mode theory [17].

All the results indicate that at low terahertz regime this device can potentially be used as a (bio) sensing platform, such as for detecting the presence of specific biological polymers such as protein etc. Nevertheless, it should be admitted that the sensitivity level found in this study is relatively low.

4. Summary

We have discussed the transmission characteristics of a microscale dielectric slab waveguide device with a deep groove and an embedded metallodielctric grating. It is found that the corresponding device shows a relatively large enhancement factor at near perpendicular incident of continuous electromagnetic wave of TM mode. This phenomenon can be explained as the consequence of the existence of surface plasmon interaction of two adjacent metal-dielectric interfaces. This enhancement can be increased further by reducing the corresponding grating filling factor. Compare to the device with fully dielectric grating, this device shows a better performance. As the chosen operational frequency is at low terahertz frequency, and the device exhibits a linear response with respect to the varying analyte refractive index; therefore, it can be considered as (bio) sensing platform.

Acknowledgement

This work is supported by the Ministry of Education and Culture, Republic of Indonesia, through “Penelitian Strategis Unggulan” DIPA-IPB 0558/023-04.2.01/12/2012, under contract no. 44/I3.24.4/SPK-PUS/IPB/2012.

References

[1] M.I. Stockman, Nanoplasmonics: past, present, and glimpse into future, Opt. Express 19 (2011) 22029–22106.
[2] H. Raether, Surface Plasmons on Smooth and Rough Surfaces and on Gratings, Springer, Berlin, 1988.
[3] M. Maisonneuve, O. d'Allivy Kelly, A.-P. Blanchard-Dionne, S. Patskovsky, M. Meunier, Phase sensitive sensor on plasmonic nanograting structures, Opt. Express 19 (2011) 26318–26324.
[4] O. Krupin, H. Asiri, C. Wang, R.N. Tait, P. Berini, Biosensing using straight long-range surface plasmon waveguides, Opt. Express 21 (2013) 698–709.
[5] K. Toma, J. Dostalek, W. Knoll, Long-range surface plasmon-coupled fluorescence emission for biosensor applications, Opt. Express 19 (2011) 11090–11099.
[6] H. Yoshida, Y. Ogawa, Y. Kawai, S. Hayashi, A. Hayashi, C. Otani, E. Kato, F. Miyamaru, K. Kawase, Terahertz sensing method for protein detection using a thin metallic mesh, Appl. Phys. Lett. 91 (2007) 253901.
[7] W.T. Kung, Y.H. Pai, Y.K. Hsu, C.H. Lin, C.M. Wang, Surface plasmon assisted Cu_xO photocatalyst for pure water splitting, Opt. Express 21 (2013) A221–A228.
[8] C. Perrotton, R.J. Westerwaal, N. Javahiraly, M. Slaman, H. Schreuders, B. Dam, P. Meyrueis, A reliable, sensitive and fast optical fiber hydrogen sensor based on surface plasmon resonance, Opt. Express 21 (2013) 382–390.
[9] A. Hassani, M. Skorobogatiy, Surface plasmon resonance-like integrated sensor at terahertz frequencies for gaseous analytes, Opt. Express 16 (2008) 20206–20214.
[10] A. Karar, N. Das, C.L. Tan, K. Alameh, Y.T. Lee, Design of high-sensitivity plasmonics-assisted GaAs metal-semiconductor-metal photodetectors, IEEE Proc. 138 (2010) 19–21.
[11] M.W. Kim, T.T. Kim, J.E. Kim, H.Y. Park, Surface plasmon polariton resonance and transmission enhancement of light through subwavelength groove arrays in metallic films, Opt. Express 17 (2009) 12315–12322.
[12] B. Wang, Y. Jin, S. He, Design of subwavelength corrugated metal waveguides for slow waves at terahertz frequencies, Appl. Opt. 47 (2008) 3694–3700.
[13] U. Schröter, D. Heitmann, Surface-plasmon-enhanced transmission through metallic gratings, Phys. Rev. B 58 (1998) 15419–15421.
[14] J. Xu, K.W. Plaxco, S.J. Allen, Probing the collective vibrational dynamics of a protein in liquid water by terahertz absorption spectroscopy, Protein Sci. 15 (2006) 1175–1181.
[15] A. Taflove, S.C. Hagness, Computational Electromagnetics: The Finite Difference Time Domain Method, Artech House, Boston, 2000.
[16] Y. Todorov, L. Tosetto, J. Teissier, A.M. Andrews, P. Klang, R. Colombelli, I. Sagnes, G. Strasser, C. Sirtori, Optical properties of metal-dielectric-metal microcavities in the THz frequency range, Opt. Express 18 (2010) 13886–13907.
[17] J. ČtyrokÝ, F. Abdelmalek, W. Ecke, K. Usbeck, Modelling of the surface plasmon resonance waveguide sensor with Bragg grating, Opt. Quantum Electron. 31 (1999) 927–941.